

# Short Range Radar Observations on Ekströmisen, Antarctica

By Andreas Rosenberger<sup>1</sup>, Hans Oerter<sup>2</sup> and Heinz Miller<sup>2</sup>

**Summary:** A new digital impulse radar was designed at Alfred Wegener Institute in cooperation with the department of high-frequency engineering of the Technical University of Hamburg-Harburg and has undergone a first field-test on the Ekströmisen. Due to a special dynamic compression scheme the instrument has excellent short range capabilities and the resolution is better than one meter. Several profiles were acquired during the tests in the austral summer season 1992-1993 from which examples are given here. The longest profile covers 60 km starting from Halvfarryggen down to the central part of the Ekströmisen and continues north towards the German wintering-over base Neumayer Station. Although the data quality of the long range record suffered from electromagnetic compatibility problems which could not be immediately remedied in the field, the short range records show detailed structure which may give some insight into the flow kinematics of the Ekströmisen.

**Zusammenfassung:** Am Alfred-Wegener-Institut wurde in Zusammenarbeit mit dem Lehrstuhl für Hochfrequenztechnik der TU Hamburg-Harburg ein neues digitales Impulsradar entwickelt und auf dem Ekström-Eisschelf getestet. Das Gerät ist mit einer speziellen Dynamik-Kompression ausgestattet, zeichnet sich durch eine hohe Auflösung in der Vertikalen aus und ist besonders für flachgründige Untersuchungen geeignet. Während der Feldsaison 1992/93 wurden einige Profile vermessen, die beispielhaft vorgestellt werden. Das mit 60 km längste Profil verläuft vom Halvfarryggen über das zentrale Ekström-Eisschelf nach Norden zur Neumayer Station. Die beobachteten Radargramme zeigen für die obersten 100 m detaillierte Strukturen, die Rückschlüsse auf Fließstrukturen im Schelfeis ermöglichen; für die größeren Eindringtiefen litten die Ergebnisse unter technischen Problemen, die erst unter Feldbedingungen zutage traten.

## 1 INTRODUCTION AND DESCRIPTION OF THE INSTRUMENT

Our radar instrument follows the concept of an impulse radar where a short voltage-pulse is transmitted and returns are received through broad-band dipoles. It is a conventional system and we benefited from the fact that some components have become available „off the shelf“ due to an expanding market for geotechnical radars which employ the same principle.

Our transmitter is a commercially available avalanche circuit (GSSI 788) which generates 5 kW peak pulse-power into a 200 Ohm resistive load with a pulse-width of about 2 ns.

The antenna pairs were built as resistively loaded dipoles according to the well known Wu-King design (WU & KING 1965) from flexible insulated copper wire. Continuous resistive load-

ing is approximated by fitting resistors into the antenna at equidistant intervals.

As there is an inherent trade-off in band width versus efficiency of the antenna on the one hand and increasing attenuation of electromagnetic waves in ice towards higher frequencies on the other, the usable frequency-band was split into two sub-bands covered with antenna sets of 30 MHz and 100 MHz nominal center-frequencies to allow for long range/low resolution and short range/high resolution experiments, respectively.

The receiver design was carried out at the department of high-frequency engineering of the Technical University of Hamburg-Harburg. With respect to the dynamic range requirements design efforts were directed to limit the impact of the direct coupling air and snow waves which would otherwise saturate the following receiver circuits and mask short range reflections. From the schematics in Fig. 1 it can be seen that this is accomplished by feeding the received signal through a so-called MMIC-attenuator switch which changes its attenuation characteristics from near 0 to about -50 dB within a switching time of 3 ns. This switch is triggered during the reception of the direct coupling wave and protects the sensitive receiver circuitry. A following bank of attenuators provides gain-ranging capabilities as it can be switched under computer control in steps of -4 dB from zero up to a maximum attenuation of -56 dB during one transmission cycle. In this way a time-range dependent step-like gain curve may be created to compensate for spherical spreading, scattering and absorption losses of late returns. A 33 dB multistage low-noise amplifier is the last link to the output of the receiver.

Digitization is carried out in two steps. We employ a sampling-oscilloscope module Tektronix 7S14 to sample the signal in equivalent time. Here a single sample with successively increasing delay (the sample interval) is taken from a single experiment and the experiment has to be repeated until the required time-range has been sampled. The 7S14 module allows for equivalent-time sampling rates up to 3 GHz and outputs discrete analogue voltage values at a repetition rate of 25 kHz which - after matching signal levels - are synchronously fed to a 12 bit A/D-converter (Keithley DAS-1602 PC plug-in board).

In the actual field set-up the main unit comprising an industry-standard 386 computer with external 450 MB SCSI hard-disk, a ruggedized thermal printer-plotter (RMS-Instruments) and the circuitry for timing and digitization is built into a 19" shock-mounted chassis within a water-protected case. The main unit,

<sup>1</sup> Dr. Andreas Rosenberger, Alfred Wegener Institute for Polar and Marine Research, now University of Bremen, Department of Geosciences, P.O.Box 330440, D-28334 Bremen

<sup>2</sup> Dr. Hans Oerter and Prof. Dr. Heinz Miller, Alfred Wegener Institute for Polar and Marine Research, P.O.Box 120161, D-27515 Bremerhaven

Manuscript received 23 February 1996; accepted 14 June, 1996

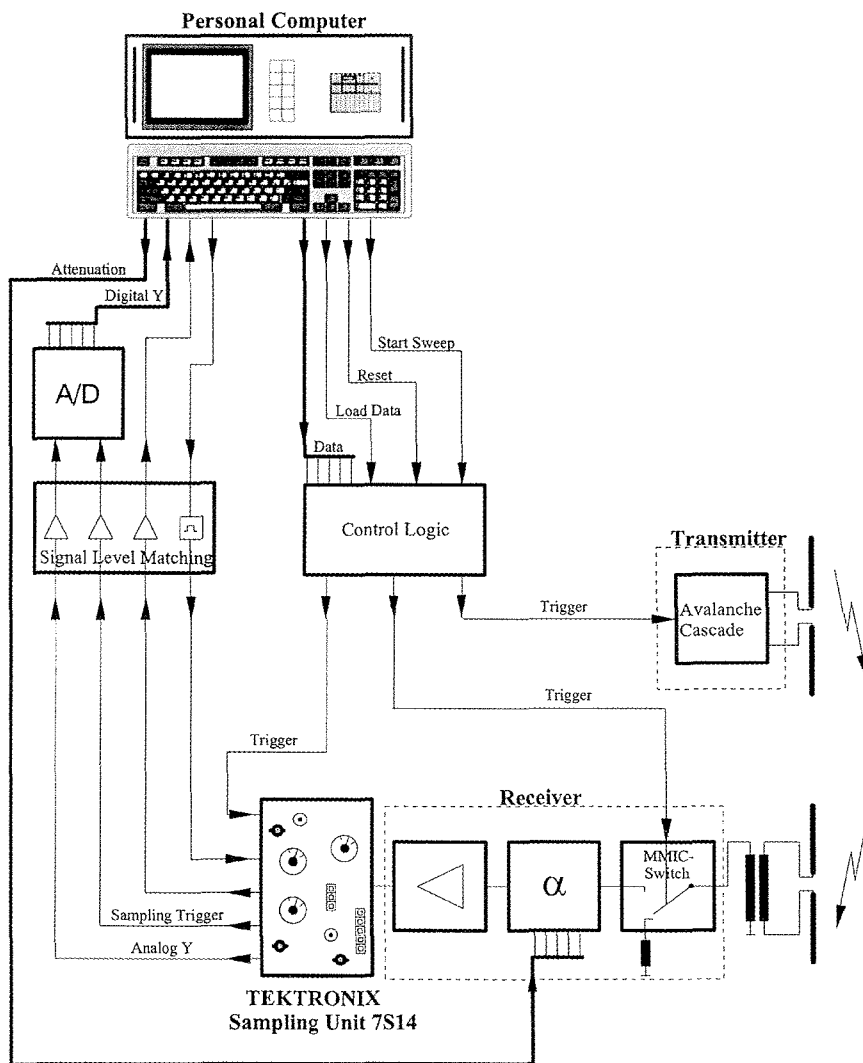


**Fig. 1:** Schematic diagram of the ice-radar instrument. Effective short-range recordings depend on the ability to attenuate the direct coupled waves. This is accomplished by the MMIC-switch which is triggered by the computer and attenuates the direct coupled waves by 50 dB thus protecting the pre-amplifier from saturation. A following bank of attenuators also controlled by the computer provides a means to establish a time dependent gain-curve.

**Abb. 1:** Blockschaubild des Eisradars. Für eine effektive Nahfeldbeobachtung muß das sehr starke direkte Signal ausgeblendet werden. Dies wird durch den MMIC-Schalter erreicht, der rechnergesteuert die direkte Welle um 50 dB abschwächt und damit den Vorverstärker vor Übersteuerung schützt. Mit der nachgeschalteten, rechnergesteuerten Abschwächerkette kann eine zeitabhängige Verstärkung erzielt werden.

two 12 V, 120 Ah car batteries, a small gasoline generator used to recharge the batteries and a box for spares fit on a Nansen sled which also carries an odometer wheel which is periodically read by the computer. The sled is towed by a snow scooter and the receive and transmit antennas trail behind on wooden racks fitted with cross-country skis in distances of 2 and 10 m, respectively. Generally no operator interference is required once the instrument has been set up, the computer screen and the plotter provide on-line records of the profile.

Estimated performance data for our radar are given as below

Transmitter output power (peak)	5 kW
Noise level (laboratory conditions)	-56 dBm
Dynamic range (field configuration)	83 dB
Sensitivity	123 dB
Digital precision	114 dB (floating point)
Maximum range (30 MHz antenna, cold ice, -12 dB reflecting bed-rock)	≈ 1000 m

Maximum range for the 30 MHz dipole-set was estimated from the radar-equation as given in WRIGHT et. al. (1990) using the same parameters as the authors i.e. we assume an antenna gain

of 1.64, an antenna efficiency of 10 %, a -12 dB specular reflecting target and a transmission loss of 0.01 dB/m. Performance of the instrument during this survey was substantially degraded due to noise leaking in behind the attenuator-bank. This problem could not be remedied in the field.

## 2 PROFILES FROM EKSTRÖMISEN

Several profiles were acquired during the austral summer-season 1992/1993 in the vicinity of the German wintering-over base Neumayer in Antarctica and during a six day trip southbound to the Olymp and Watzmann remote seismic observatories on Søråsen and Halvfarryggen (Fig. 2). A comprehensive study of ice thickness of the Ekstömisen Ice-Shelf was carried out by THYSSEN & GROSFELD (1988) by airborne radar-surveys in 1981, 1984 and 1986.

## 2.1 From the Neumayer Station to the old Georg v. Neumayer Station

Two data examples are given in Figs. 3 and 4. The profile in Fig. 3 runs from the new wintering-over base Neumayer Station northwest over 7 km towards the recently abandoned old base Georg v. Neumayer Station (G.v.N., Fig. 2, Line C). The 100 MHz antenna pair was used and the distance between traces averages 10 m at an average progress along the profile of 6 km/h.

Data are sampled with a pre-trigger, the avalanche transmitter fires about 390 ns after A/D conversions start. The first break at  $0.42 \mu\text{s}$  marks the arrival of the direct coupled air-wave. This timing puts the first break at the very edge of the first 500 ns digitization window which has the advantage that receiver-attenuation can be reset immediately after the first break decays.

Transmitter and receiver antennas are 10 m apart but the setup for trailing the wooden antenna platforms is not rigid. Consequently small changes in receiver-transmitter distance introduce jitter in signal onset and also the geometry of the travel path for reflections is slightly altered. Near surface reflections are of course more affected than reflections with longer travel times.

Over the whole length of the profile the bottom return is clearly visible and, assuming an average propagation velocity of  $170 \text{ m}/\mu\text{s}$  ice thickness decreases toward the northwest (shot 1) from an initial 220 m ( $2.58 \mu\text{s}$  two-way traveltime) to about 190 m ( $2.24 \mu\text{s}$  two-way traveltime) in the vicinity of the G.v.N. station (shot 800). Fig. 4 shows a close-up of the first  $0.7 \mu\text{s}$  of the record between shots 450 and 800, clearly coherent events can

be traced down to  $0.68 \mu\text{s}$  gently dipping down towards the northeast.

With regard to the limitations in resolution one has to bear in mind that these signals are likely to be a composite pattern of interference from single reflections rather than being a direct representation of the individual discontinuities in impedance themselves. General difficulties with the interpretation of short-range ice-radar records arise as well from the probable presence of multipath returns. The autocorrelation function of a record provides no proof either for the presence or for the absence of multiple reflections when the targets themselves form a quasi-periodic pattern. In section 3 some general considerations with respect to the interpretation of short range radar records are discussed in more detail.

The origin of these near surface reflections is not clear and it remains an unresolved issue whether reflections from the firn column are generated by density- or conductivity contrasts. The firn-ice boundary in that area on the Ekströmsisen is generally found at a depth not greater than 50 m. A decreasing volume content of air in individual firn layers does not give rise to sharp impedance contrasts which would in turn be required to generate equally sharp reflections. Compaction of snow is a more gradual process and, what is more, does not necessarily preserve the layers of deposition when accumulation rates vary locally. On the other hand melting and percolation during the summer season is common on Ekström and traces thereof can be seen in the walls of snow-pits in the form of lenticular inclusions of clear ice in the firn. These ice-lenses exhibit a thickness in the order of several centimeters and a horizontal extension in the order of meters, more like a pattern of individual frozen pudd-

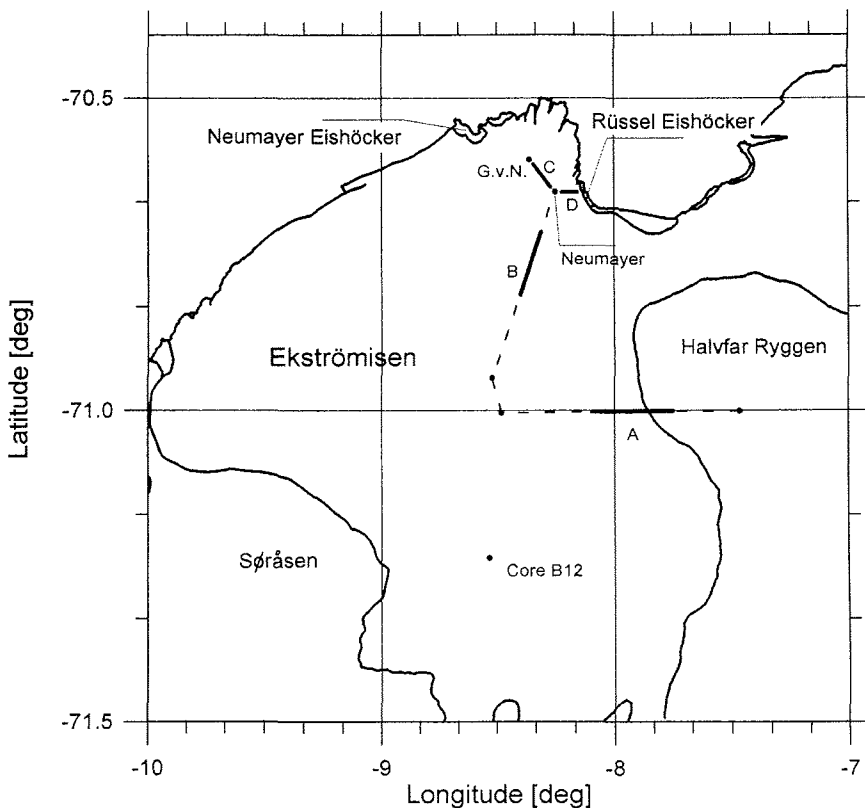


**Fig. 2:** Map of Ekströmsisen after IFAG (1989). G.v.N. denotes the old Georg-von-Neumayer research station which was abandoned in 1992. The German observatory moved to Neumayer Station. The dashed line with solid segments A and B marks the longest radar profile acquired, subsets of the data from segments A and B are presented in Figs. 7 and 9.

**Abb. 2:** Karte des Ekström-Eisschelfs nach IFAG (1989). G.v.N. markiert die Position der alten Georg-von-Neumayer-Station, die 1992 aufgegeben wurde. Die gestrichelte Linie zeigt das längste kontinuierlich beobachtete Profil. Ausschnitte aus den fett markierten Segmenten A und B werden in den Abb. 7 und 8 dargestellt.

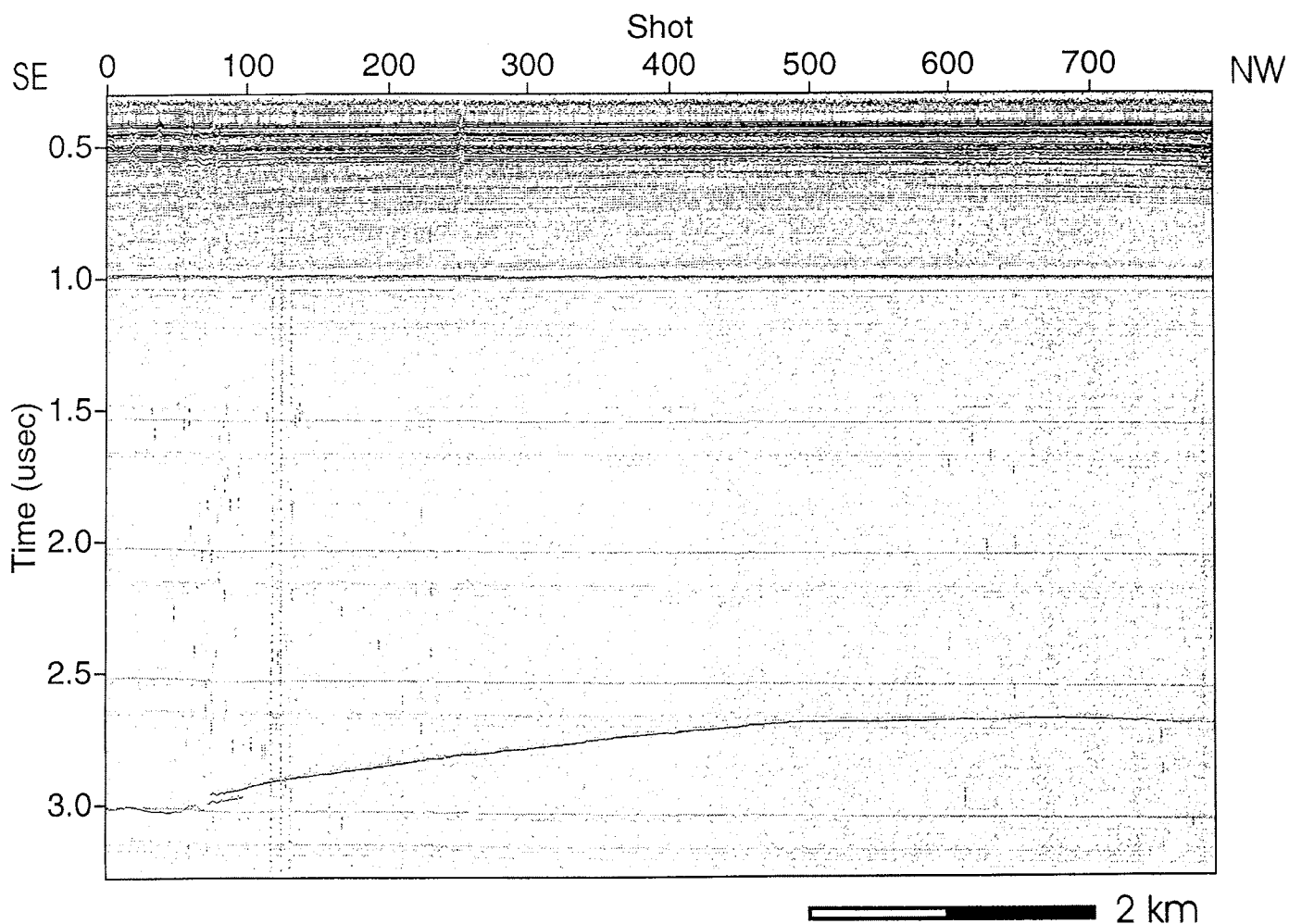


**Fig. 3:** Profile running from the new Neumayer Station (Shot 0) to G.v.N. over a distance of 7 km. It was acquired using 100 MHz antennas. The bottom reflection is visible as a thin line running from 3  $\mu$ s at shot 1 to 2.6  $\mu$ s at shot 800.

**Abb. 3:** Dieses 7 km lange Profil führt von der neuen Neumayer Station (Schuß 0) zur G.v.N.-Station und wurde mit einer Signalfrequenz von 100 MHz beobachtet. Die Reflexion von der Unterseite des Schelfeises ist als dünne Linie sichtbar und verläuft von 3  $\mu$ s am Schußpunkt 1 nach 2.6  $\mu$ s am Schußpunkt 800.

les sunken into the firn, and as such are more likely to scatter electromagnetic energy in the spectral band under discussion than to generate coherent reflections extending over hundreds of meters. Under the assumption that reflections are caused by properties of deposition at a common instant in time, this leaves as an alternative the hypothesis that reflections are generated by abrupt changes in permittivity introduced by salty or acid horizons as the more likely one. The seasonal break-up of the near sea-ice occurs within a few weeks, fast enough for the salty sea-spray carried in by the wind to generate sharp contrasts in permittivity uniformly over a wide area. In fact, as investigations near the G.v.N. station have shown (GÖRLACH et al. 1985), prominent peaks in salinity occur in the austral autumn, March through June, when the sea is still open and high winds prevail. A depth profile in a 50 m firn core taken by the same authors shows pronounced individual peaks of as much as 90 mg/kg salt down to a depth of about 27 m, after which salinity decreases abruptly by two orders in magnitude. GÖRLACH et al. (1985) argue that the firn in that depth has been carried in from the south over a distance of about 7 km along the flow-line to its present position and conclude that the immediate strong influence of

salty aerosol is limited by a sharp boundary south of the coastline.

These observations agree quite well with what can be seen in Fig. 4 where the last detectable reflector shows at 0.7  $\mu$ s (0.29  $\mu$ s two-way-traveltime) which translates to a depth of about 25 m.

Our observations are further supported by data from two 10 meter cores which were retrieved in 1987 (MILLER & OERTER 1990) at locations along the main southbound trail at distances of 2 km and 40 km south of the G.v.N. observatory. In both cores (Fig. 5) a series of very prominent peaks in conductivity relating to seasonal events can be seen. It may further be noticed that conductivity generally decreases two orders of magnitude from one location to the other. Density data from both cores in Figure 5 do show a more steady behaviour, the two density-peaks in between a depth of 6-8 m in the core from KM 2 are local features and due to the above mentioned partial melting- and percolation-process.

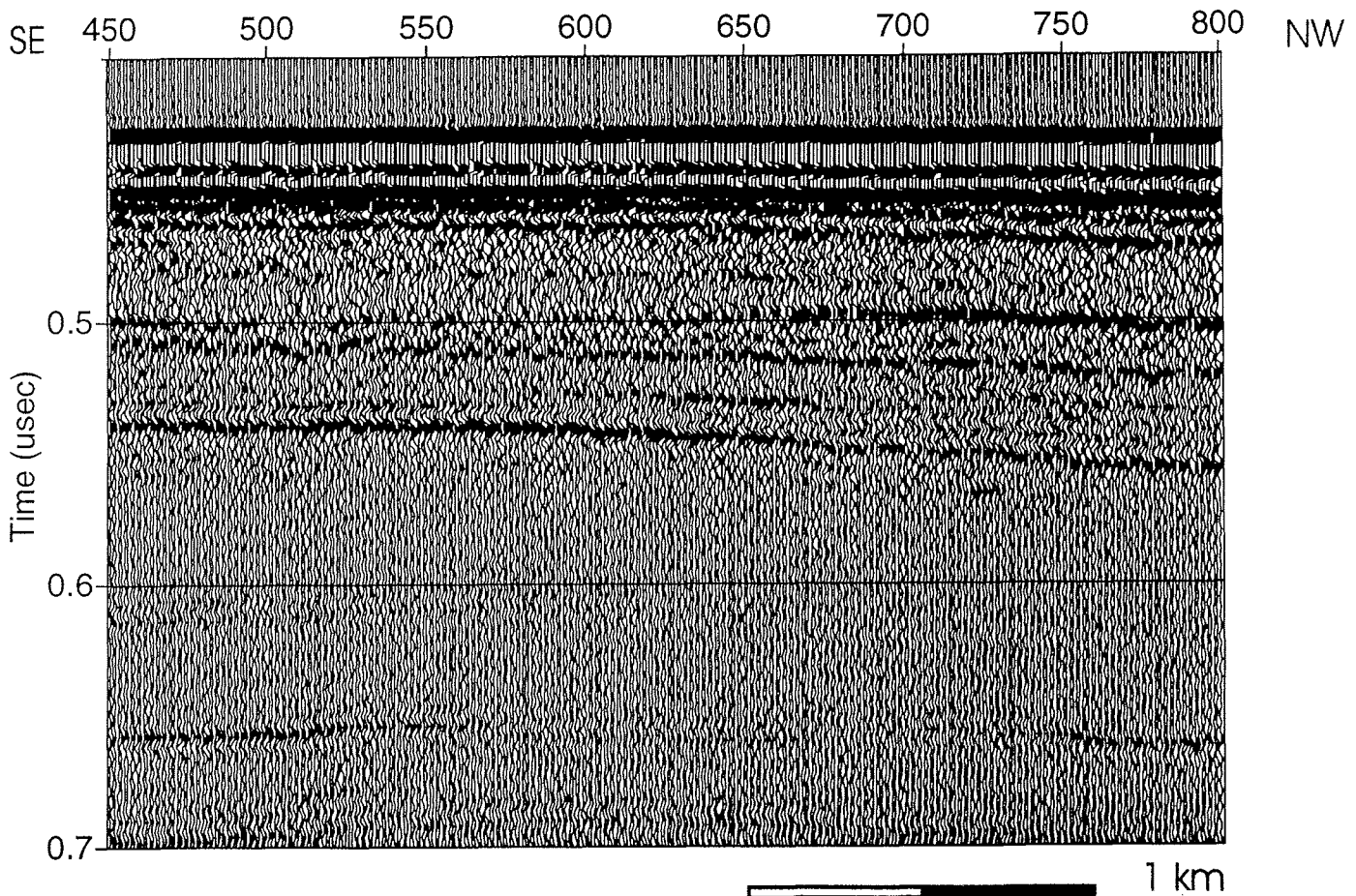


**Fig. 4:** Enlarged near surface record of a subset of traces shown in Fig. 3. Near surface reflections down to  $0.66 \mu\text{s}$  are most probably caused by seasonal variations in salinity. A salt content peaking up to  $90 \text{ mg/kg}$  has been found in cores taken in the vicinity of the G.v.N. station. Salt content decreases by two orders in magnitude in depths greater than 30 m.

**Abb. 4:** Ausschnitt aus Abb. 3. Oberflächennahe Reflexionen bis zu einer Laufzeit von  $0.66 \mu\text{s}$  sind sehr wahrscheinlich durch saisonale Änderungen der Salinität des Firns bedingt. In Eiskernen aus der Umgebung der G.v.N.-Station wurden Salzgehalte bis zu  $90 \text{ mg/kg}$  gefunden. In Tiefen größer als 30 m ist der Salzgehalt um zwei Größenordnungen niedriger.

## 2.2 Rüssel-Eishöcker

The section shown in Fig. 6 is part of a profile running from the Rüssel Eishöcker (shot no. 1) west towards the Neumayer Station (Fig. 2, line D). The Rüssel Eishöcker and Neumayer Eishöcker northwest of the Neumayer Station are the topographic expressions of two major obstructions to ice-flow, the ice-shelf is grounded in both areas. We had to give up our original intention to run the profile onto the grounded part of the ice-rise as more and more firn-covered crevasses became apparent to the naked eye. Many crevasses which we were not even aware of had already left their clear imprint in the radar record as diffraction hyperbolas close to the surface as well as in the bottom reflection. Presumably the whole ice-body is broken at some places forming huge A-shaped crevasses like the one appearing as a gap in the bottom reflection flanked by diffraction hyperbolas around trace 150. Here the 30 MHz antennas were used, the distance between traces is about 5 m acquired at a profiling speed of 3 km/h. The profile section in Fig. 6 covers a distance of about 1000 m running east to west.

Although barely visible in Figure 6, the near surface record in

the undisturbed part of the firn further west towards the Neumayer Station (from shot 200 on) exhibits a structure of reflections comparable to those discussed above. In relation to the diffraction amplitudes originating from firn/air interfaces these reflections are much weaker and do not show up well in a grey-scaled plot.

Attempts to focus near surface diffractions by migration based on a velocity function as given in BLINDOW (1986) show that many hyperbolas do not collapse. This is most probably due to the fact that the corresponding diffractions originate off track which in turn is an indication that the profile does not run perpendicular to the strike of the crevasses.

## 2.3 Halvfar West Flank

The section in Fig. 7 is part of the longest profile acquired during the tests. The profile was run westbound along the marked trail leading down from the Halfvar ice-rise over the presumed grounding line onto the Ekströmsen, then turning North and terminating about 10 km short of the Neumayer Station. The part

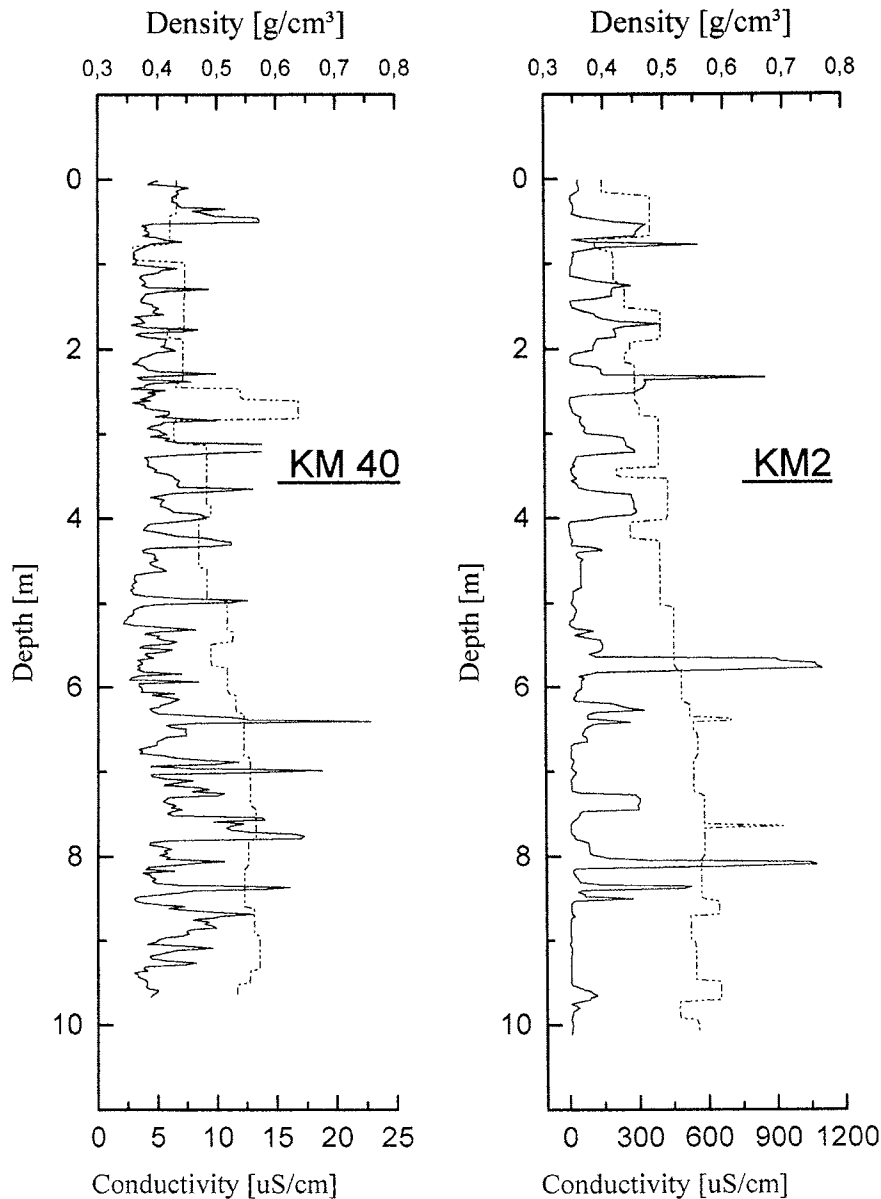


**Fig. 5:** Conductivity and density logs from two 10 m cores taken from locations in distances of 2 km and 10 km south of G.v.N. station in 1987. Solid lines are conductivity. The general trend that conductivity drops two orders in magnitude as one moves away from the coast can be read from the scale of the conductivity axis. Peaks in conductivity are related to seasonal storms which distribute sea-spray from the open sea over large distances inland. Peaks in density on the other hand are local features only. During the summer season partial melting occurs at the surface and percolation forms ice-lenses with lateral extensions in the order of meters only.

**Abb. 5:** Leitfähigkeits- und Dichte-Tiefenverteilungen an zwei 10 m langen Eiskernen, die in 2 und 10 km Entfernung südlich der G.v.N.-Station erbohrt wurden. Die durchgezogenen Linien zeigen die Leitfähigkeit und deren abnehmenden Trend mit zunehmendem Abstand von der Küste. Spitzen in den Leitfähigkeitskurven korrespondieren mit saisonalen Stürmen, die Salz aus dem offenen Meer bis weit in das Inland verfrachten. Spitzen in den Dichteverteilungen sind nur lokale Phänomene. Sie sind bedingt durch Schmelzvorgänge in der Schneedecke während des Sommers mit nachfolgender Bildung von lateral begrenzten Eis-linsen.

of the track corresponding to Fig. 7 is highlighted in Figure 2, the section shown corresponds to part A. Total distance covered is about 62 km with an average distance between shots of about 20 m. Due to high background noise the reflection from the ice-rock interface, and even more interesting, the transition over the grounding-line did not leave a detectable signal in the records. The bottom reflection reappears at about 4.8  $\mu$ s TWT in the data far in the northern leg of the profile when ice thickness has decreased to about 410 m. However, all along the profile the near surface record up to 1.3  $\mu$ s (0.9 ms TWT) again reveals structure, coherent over several tens of kilometers. Fig. 7 shows a subset of the data acquired crossing over the presumed grounding-line.

The sudden change in the signal characteristics of the direct wave shortly after shot 600 is due to the fact that the sled carrying the transmitter got tangled in the towing rope and the antenna was rotated with respect to the receiver antenna. This problem was corrected shortly after shot 700. Fortunately reflected signals are not affected. From 1.0  $\mu$ s on attenuation is reset by

20 dB, the reconstruction of amplitudes elevates the level of noise which is leaking in behind the attenuators. The line appearing at 1.0  $\mu$ s is trigger cross-talk.

Again the wave-like structures represent an interference pattern as traveltimes differences between neighbouring signals are at the very limit of the instrument's resolution capabilities and multipathed signals are probably present. Nevertheless this pattern is still representative for the general behaviour of reflectors horizontally along the track which is indeed remarkable.

Similar internal structures have been observed on Ice-Stream B, West Antarctica by WRIGHT et al. (1990). They suggest that these structures may originate from „island or rafts of ice“ which have been incorporated into the stream or may as well be generated as an artifact due to side-reflections from „healed“ crevasses in a varying horizontal distance from the profile track. Both interpretations are not suitable for the situation here.

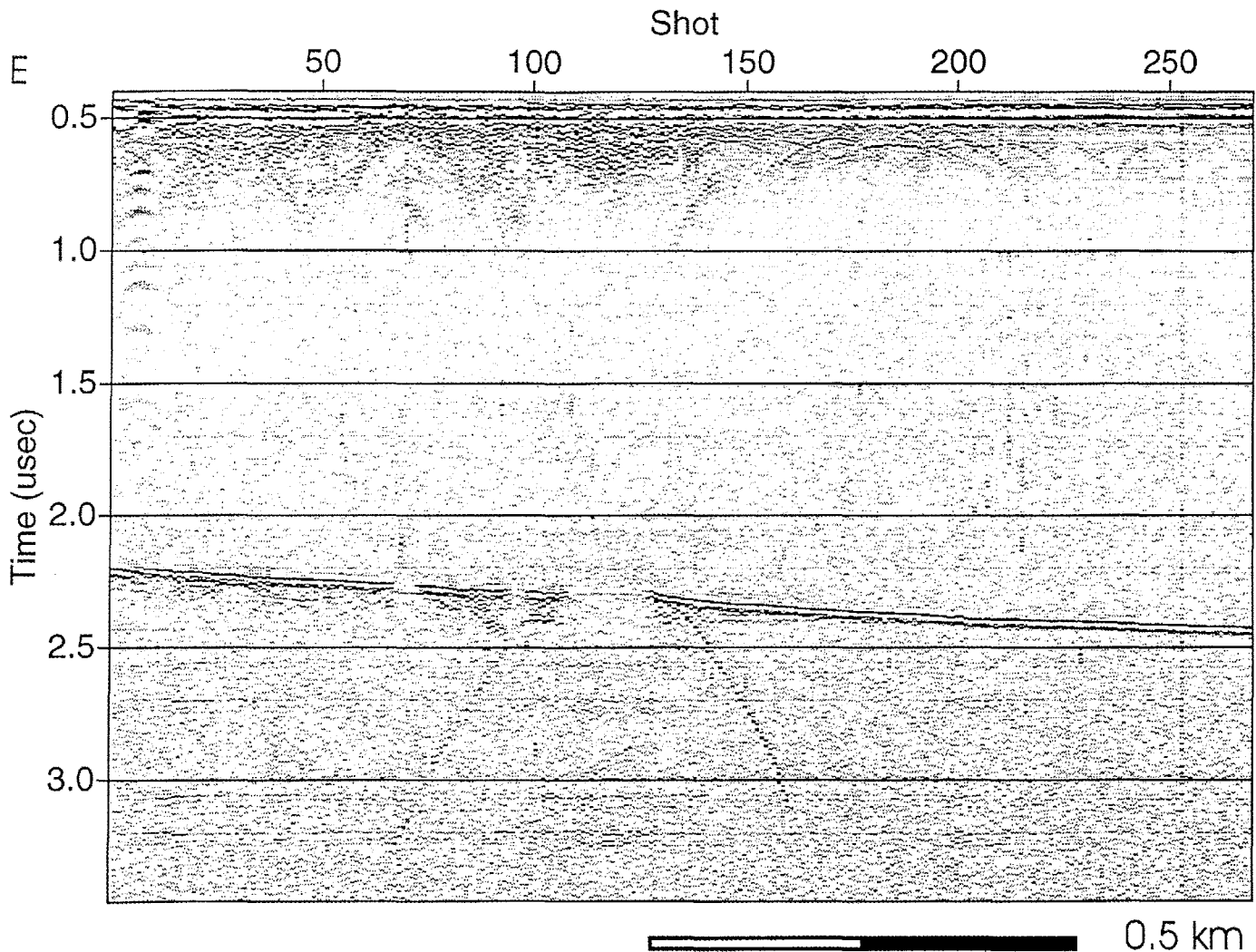


**Fig. 6:** Section of a profile running east (left side) to west from the Rüssel Eishöcker towards the Neumayer Station. Crevasses produce diffraction hyperbolas close to the surface as well as in the bottom reflection between shots 100 and 150.

**Abb. 6:** Profilausschnitt zwischen Rüssel Eishöcker und der Neumayer Station. Die Diffraktionshyperbeln nahe der Oberfläche und an der Unterseite zwischen den Schußpunkten 100 und 150 sind durch Spalten verursacht.

According to our conclusion the wave-like structure in Fig. 7 is in fact a feature of deformation across the grounding-line. Slopes get steeper with depth and the magnitude of the excursions increases indicating that the deformation process is continuous, thus leaving a stronger imprint on the older material while younger firn close to the surface is hardly affected.

To support our hypothesis with respect to the origin of the reflections we present conductivity- and density-data down to a depth of 140 m from Core B12 (Fig. 8, left panel), a core with a total length of 205 m recovered in 1987 at a distance of 70 km south of the G.v.N. station (Fig. 2). Again the most pronounced events are documented in the electrolytical conductivity log with peaks up to 170 mS/cm and 100 mS/cm at depth of 16 m and 99 m respectively. This core is located some 30 km further South of our profile-leg and accordingly data from this core cannot be directly correlated to the radar observations. Still, the general properties will hold for the region. According to observations by MOSER (1991), magnitudes of chloride concentrations decrease

exponentially with distance from the coast so we can expect even higher average conductivity values at the site of the profile under discussion.

We speculate that while the ice crosses over the grounding line the ice-sheet is deformed by the interaction of inertia and buoyancy-forces as well as changes in the strain regime. While the ice sheet is frozen to the basement-rock where it is still grounded it becomes free floating once buoyancy forces lift it off the rock thus causing an abrupt and discontinuous change in the strain regime. Deformation is continuous in time and almost stationary in space. A depression is created at the surface which in turn attracts a local peak in accumulation which keeps the surface level. We see the minima of the predominant wave wander downstream (to the right in Fig. 7) only slightly with increasing depth and, as distance from the grounding line increases, relaxation of strain dampens the excursions and local variations in accumulation smooth the surface.

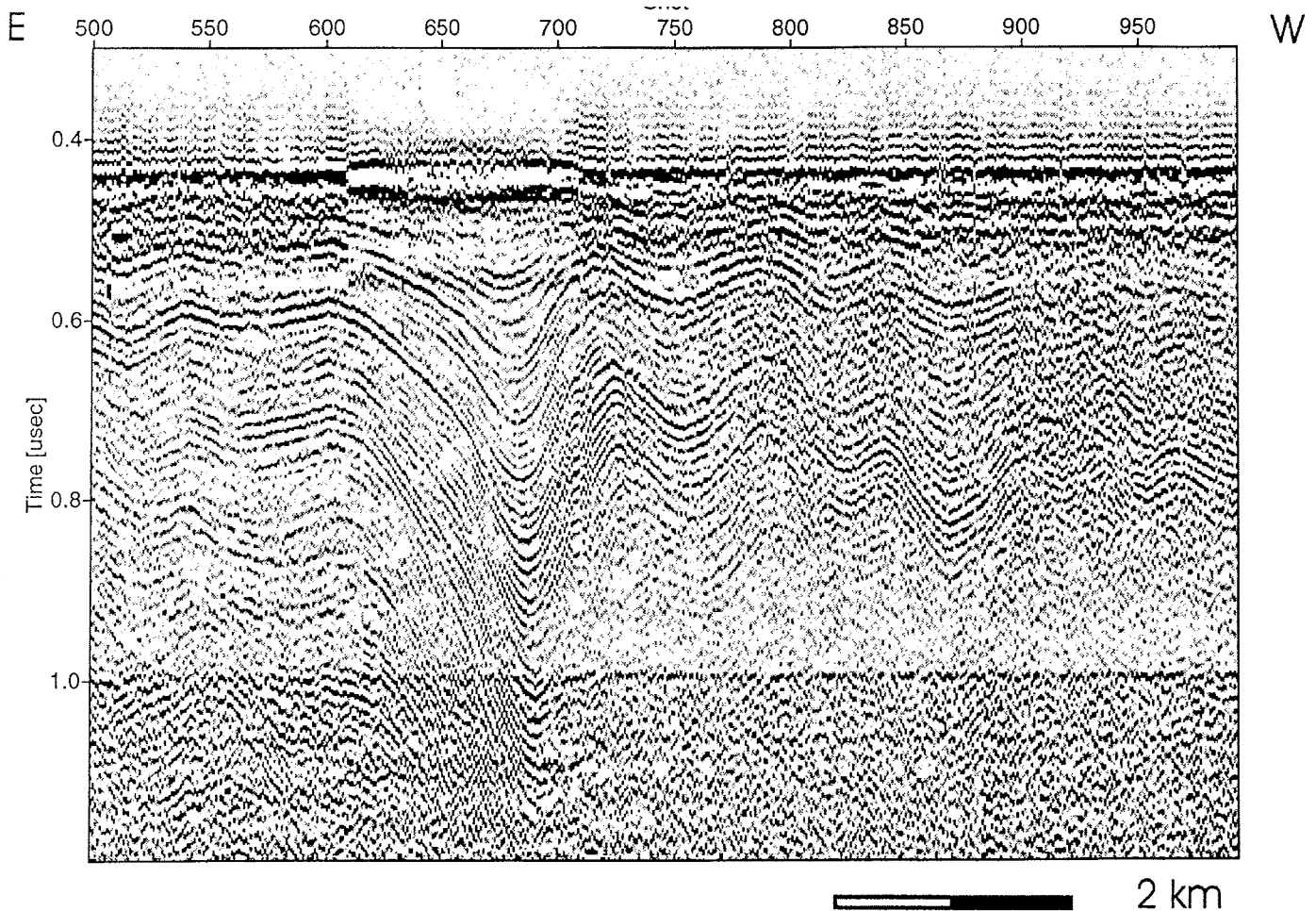


**Fig. 7:** Profile section running down from Halvfär over the grounding line (Fig. 2, section A). Internal reflections between shots 600 and 750 reveal a coherent wave-pattern. If this were a surface-induced feature created by a local accumulation pattern, deeper disturbances would wander downstream relative to near surface disturbances. This is obviously not the case so we conclude that this wave-pattern is created by a stationary deformation process at the grounding line. Vertical exaggeration is approximately 20.

**Abb. 7:** 20-fach überhöhter Profilausschnitt am Übergang vom Halvfär-Ryggen zum Schelfeis (Abb. 2, Teilstück A). Die internen Reflexionen zwischen den Schußpunkten 600 und 750 zeigen ein kohärentes Wellenmuster. Wenn dieses durch lokale Variationen in der Akkumulation bedingt wäre, dann müßten die tiefergelegenen Wellen stromabwärts versetzt sein. Da dies nicht der Fall ist, schließen wir, daß dieses Muster durch ein stationäres Deformationsfeld an der Aufsetzlinie hervorgerufen wird.

At the very end of the profile (Fig. 2, line B) between shots 3200 and 3300 (Fig. 9) we see a similar wave-pattern in the firm - although with smaller vertical amplitudes - which we think is reflecting deformation due to the obstructions to flow created by the Neumayer and Rüssel Eishöcker or may depict remnants of earlier deformations of the ice-sheet.

#### 2.4 Downstream

Several groups of reflections which we picked up on the lower west-flank of Halvfär can be traced all the way down to the end of the profile. For easier display we picked three prominent events from the turning point of the profile on the ice shelf in the north towards the very end (Fig. 10). Distance is given from the beginning of the profile, traveltimes are given as they appear in the record, so the surface (dashed line) is located at 0.42  $\mu$ s.

The general trend of the reflections to dip towards the north agrees with the fact that we move in the general direction of flow along the profile, which has been compiled by IFAG (1989) and is in the order of 130-150 m/yr. As we lack firm-density data and velocity/depth profiles, an estimate of average accumulation rates along the profile cannot be obtained. However, all three reflectors show a coherent trend in their traveltimes over distance and once again we observe that reflectors in greater depth also exhibit the most pronounced depth variations over a given distance.

This clearly does not agree with a model of uniform flow and limited variations in accumulation. Compaction of snow in the firm-column should on the contrary dampen traveltimes of a single reflector in greater depth and we should see the top-most layers exhibiting the greatest amplitudes.

We suggest that accumulation is not just following a random pattern of surface wind-flow or precipitation over an almost

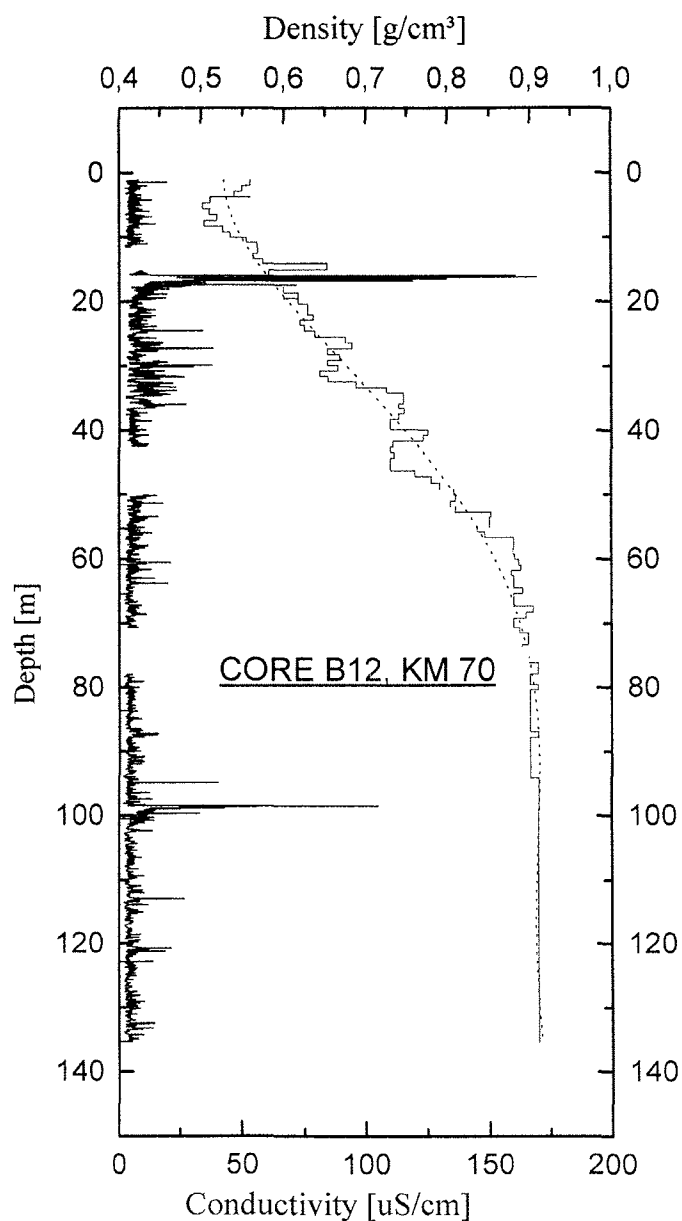


**Fig. 8:** Core B12. This 140 m long core was taken 70 km South of G.v.N. station in 1987. Shown are conductivity and density data, the dashed line is a 5th order polynomial fit to density with coefficients 0.55744, -0.47e-3, 0.31e-3, -5.2799e-6, 3.2986e-8, -7.1761e-11. Variations in conductivity are much more pronounced than variations in density.

**Abb. 8:** Verteilungen der elektrischen Leitfähigkeit und der Dichte für die oberen 140 m des Eiskerns B12. Dieser 205 m lange Eiskern wurde 1987 70 km südlich der G.v.N.-Station erbohrt. Die gestrichelte Linie gibt die Annäherung an die Dichteverteilung durch ein Polynom 5. Ordnung mit den Koeffizienten 0.55744, -0.47e-3, 0.31e-3, -5.2799e-6, 3.2986e-8, -7.1761e-11 wieder. Die Änderungen der Leitfähigkeit sind viel stärker ausgeprägt als die Änderungen der Dichte.

perfectly flat surface. Although the ice is moving towards the north these wave-like variations seem to be stationary in space rather like a stationary wave pattern of water flowing over an obstacle. Accordingly accumulation continuously straightens out the surface as it will be greatest in the troughs and smallest on the crests of such a wave.

### 3 GENERAL REMARKS REGARDING THE INTERPRETATION OF SHORT RANGE ICE-RADAR RECORDS

The bulk of research work employing radar soundings of ice bodies is focussed on establishing ice thickness which may be inferred directly from traveltimes assuming average velocities in the order of 170 m/μs for electromagnetic waves propagating in ice. Resolution - as long as the detection of a single reflection from the bottom is concerned - is not a major concern.

However, short range radar records originate partially from the region of unconsolidated firn where propagation velocity varies from close to 200 m/ms at the surface down to about 170 m/μs when firn has been transformed to clear ice. When due to changes in permittivity a complex layered structure gives rise to a pattern of reflections resolution, the ability to discriminate closely spaced events, is of major concern. Resolution depends on spectral bandwidth of the received signal only which is limited by the bandwidth of the instrument as well as the bandwidth of the transmission path.

In Fig. 11 and 12 we show examples from our data where we isolated single returns from the ice/sea-water interface at the bottom of the ice-shelf to calculate the average of 100 power-spectra for the 30 MHz and 100 MHz antenna sets respectively. The -3 dB bandwidth of the 100 MHz data is about 90 MHz while the 30 MHz return has a bandwidth of about 70 MHz. Assuming an average propagation velocity of 170 m/μs an upper bound for the resolution in each case is calculated from

$$\Delta z = \frac{c}{2\Delta f}$$

to be 0.9 m and 1.2 m for the 100 MHz and 30 MHz returns respectively. This is certainly a conservative estimate, the close range resolution may be better due to smaller absorption losses for high frequencies.

A more instructive example is given in Fig. 13, where we compare a subset of the full waveform data from the profile presented in Fig. 7 (Fig. 13, left panel) with its envelope representation (Fig. 13, right panel). The envelope of a signal calculated via the Hilbert-transform is independent of center-frequency, it depends on bandwidth only. The apparently high resolution image is degraded substantially, many events merge into a single thick envelope. This is a clear indication that many of the closely spaced events are generated by interference of single waveforms thus creating the visual impression of a high resolution record. What also can be seen in this example between shots 640 and 700 is that resolution degrades for later arrivals as one might expect as high-frequency absorption and scattering losses increase with increasing travel-time.

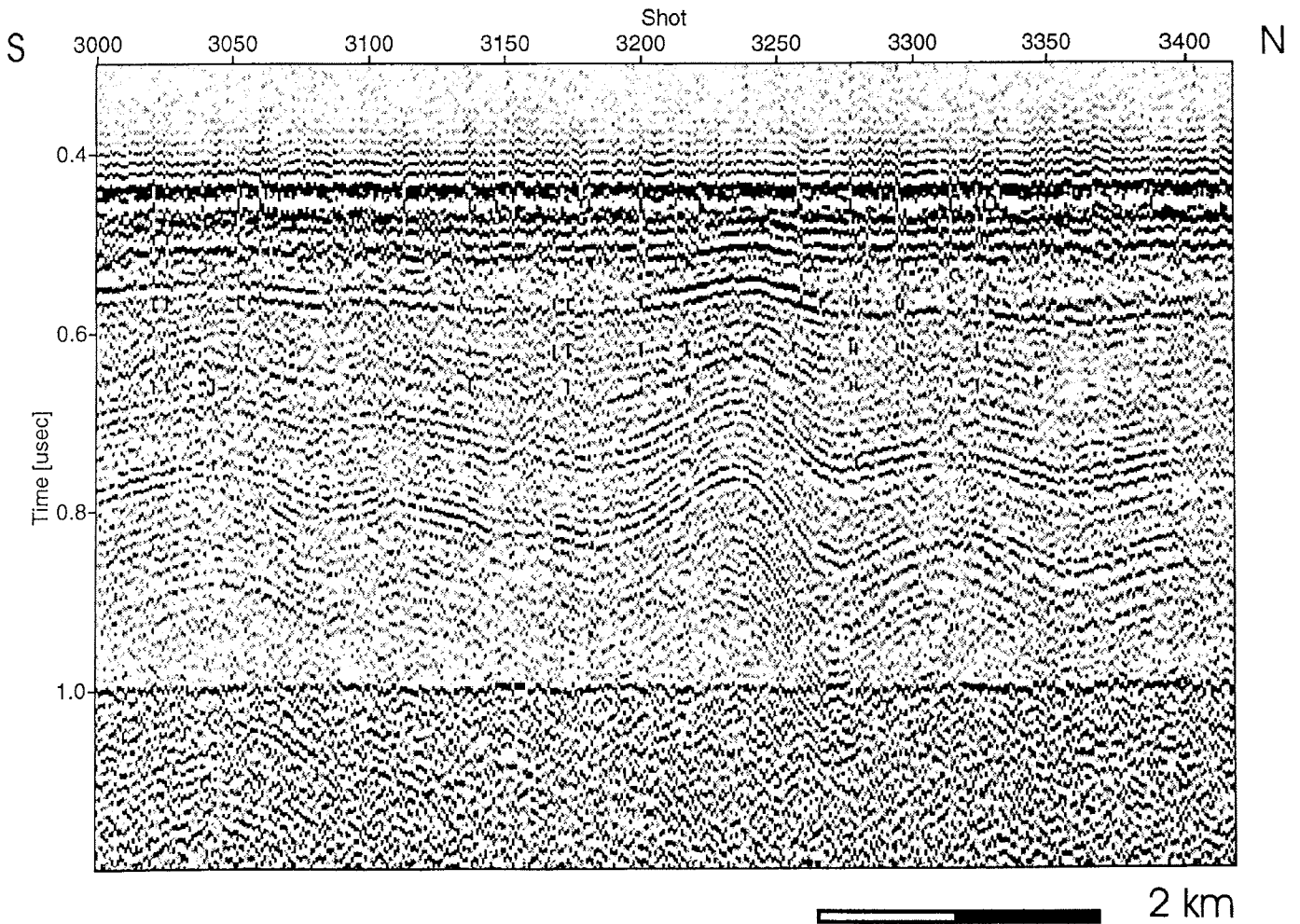


**Fig. 9:** Profile section downstream 10 km short of the Neumayer Station (Fig. 2, section B). Again a wavelike structure in the short range record indicates deformation probably due to the obstruction to flow created by the Neumayer- and Rüssel-Eishöcker. The profile runs in the general direction of flow (left to right). However, the wave-pattern does not reflect this, as crests (and troughs) of shallow as well as deep reflections occur at the same location along the profile. The deformation seems to be stationary in space.

**Abb. 9:** Profilausschnitt 10 km südlich der Neumayer Station (Abb. 2, Teilstück B). Auch hier wird eine wellenförmige Struktur beobachtet, die auf den Widerstand zurückzuführen ist, den die Neumayer- und Rüssel-Eishöcker dem fließenden Schelfeis entgegensetzen. Das Profil verläuft von links nach rechts in der allgemeinen Fließrichtung des Schelfeises. Da die Wellenberge und -täler nahe der Oberfläche und in der Tiefe an derselben Stelle beobachtet werden, muß das Deformationsfeld stationär sein.

#### 4 CONCLUSIONS

Our radar is an implementation of the most straightforward concepts with respect to signal generation and detection which nevertheless are totally adequate for a medium range system. Due to the technique employed to limit the effects of direct transmitter-receiver coupling and the provision of dynamic compression the radar provides excellent short-range records with resolution better than 12 ns.

Data from the field test clearly show that short range records can provide valuable information on relative accumulation and as well give clues to the kinematics of flow of an ice-body. Based on available data the question for the origin of short range reflections cannot be finally resolved. This is also beyond the scope of this paper. We observe continuous reflections over several kilometers and in the case of the Halvar profile in Fig. 7 from shallow depth down to the lower end of the firn column

where density contrasts necessarily have diminished. We therefore favor the hypothesis that internal reflections are related to salty horizons.

Our observation that internal reflections show significant patterns at locations coincident with a special strain regime needs to be verified, however. Modeling of ice-flow would be one way to compare flow-patterns over the grounding-line with our observation but clearly additional radar profiles in similar settings are needed.

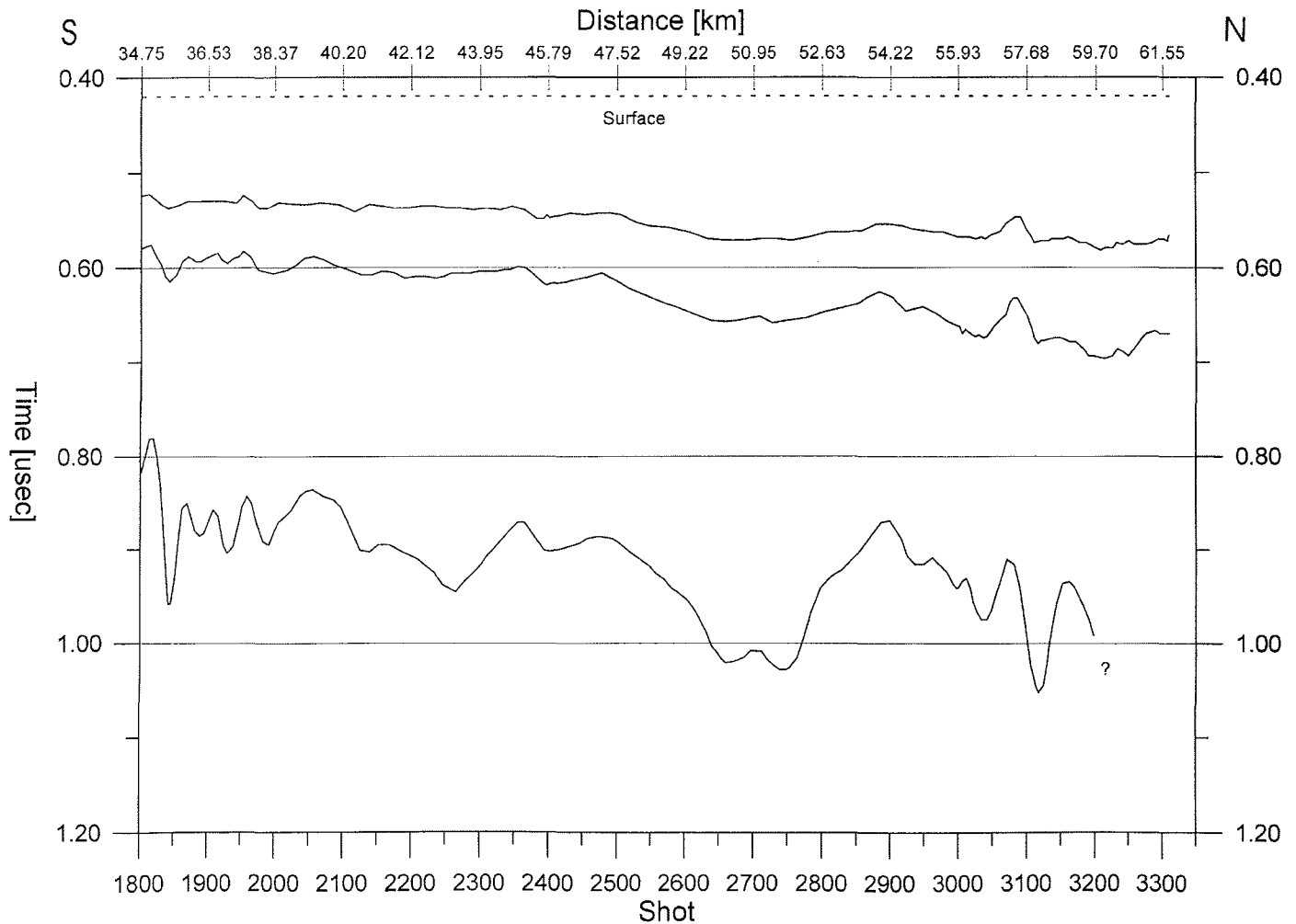


**Fig. 10:** Three prominent reflections from the downstream leg of the profile shown in Fig. 2. Reflections can be traced over a distance of 26 km and show a general dip towards the north. They also exhibit coherent behaviour with respect to traveltimes variations.

**Abb. 10:** Strichzeichnung dreier deutlicher Reflexionen beobachtet auf dem Profil aus Abb. 2. Die Reflektoren können über eine Entfernung von 26 km verfolgt werden und fallen nach Norden ein. Sie zeigen auch ein kohärentes Verhalten bezüglich der Laufzeitvariationen.

#### ACKNOWLEDGEMENTS

HF-Receiver design and detection electronics were done by J. Jelonnek and J. Winkelmann, TU-Hamburg-Harburg; system integration was carried out by B. Heesemann, Alfred-Wegener-Institute, now University of Bremen. Processing software was developed by the Colorado School of Mines, Center of Wave-Phenomena, and is as SEISMIC UNIX in the public-domain.

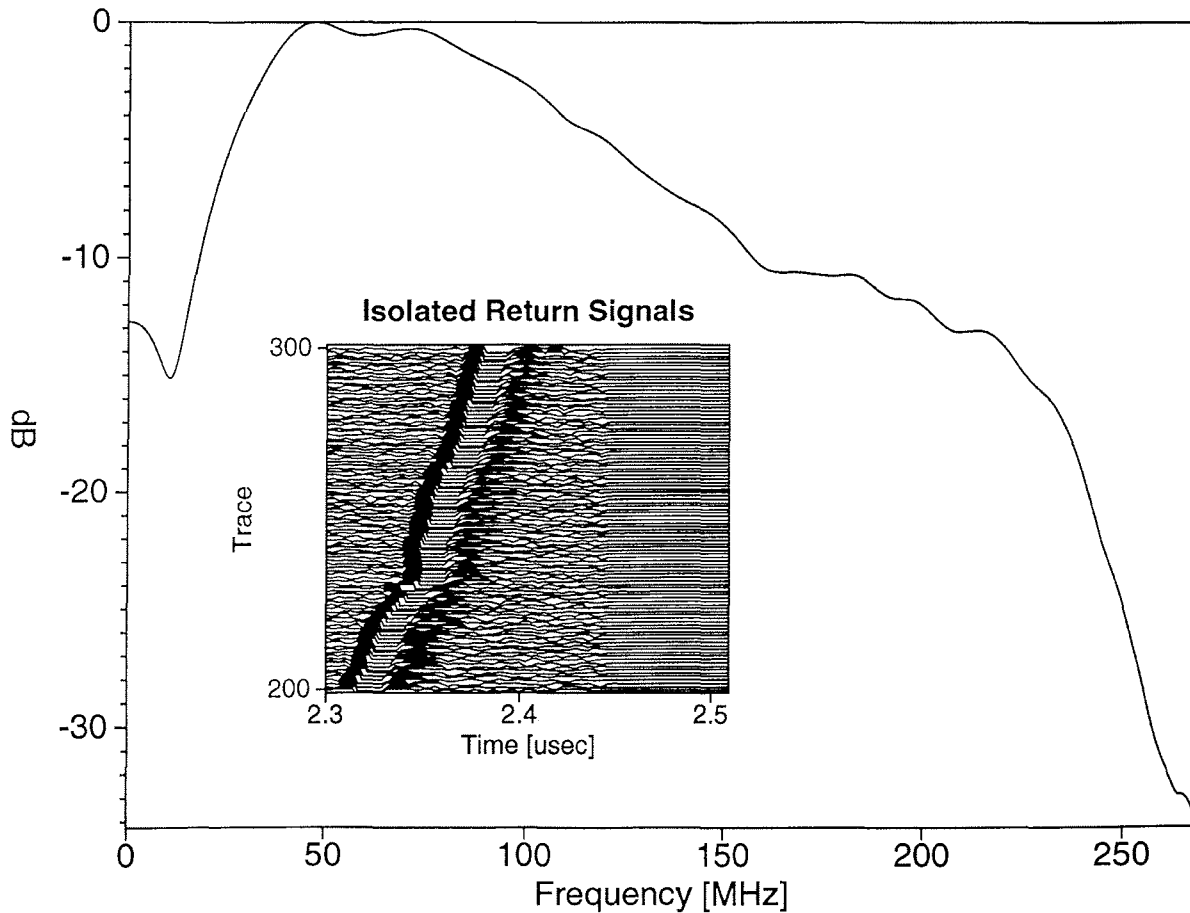


**Fig. 11:** Bandwidth of 30 MHz antennas. For an estimate of spectral bandwidth 100 spectra of the bottom returns shown in the inset have been averaged. The -3 dB bandwidth is about 70 MHz.

**Abb. 11:** Bandbreite der 30 MHz Antennen. Für die Schätzung der spektralen Bandbreite wurden 100 Spektren der Bodenechos gemittelt. Die Bandbreite zwischen den -3 dB Punkten beträgt etwa 70 MHz.

#### References

- Blindow, N.* (1986): Bestimmung der Mächtigkeit und des inneren Aufbaus von Schelfeis und temperierten Gletschern mit einem hochauflösenden elektromagnetischen Reflexionsverfahren.- Dissertation, Westfälische Wilhelms-Universität, Münster, pp. 163.
- IFAG* (1989): Ekströmisen, Map SR 29-30, Antarktis, Institut für Angewandte Geodäsie, Frankfurt a. M.
- Görlach, U. Wagenbach, D. Kipfstuhl, J. & Streckenberg, U.* (1985): Spurenstoff-glaziologische Untersuchungen an den deutschen Antarktisstationen.- Filchner Ronne Ice Shelf Progr. Report 2: 42-49, Bremerhaven.
- Looyenga, H.* (1965): Dielectric Constants of Heterogenous Mixtures.- *Physica* 31: 401-406.
- Miller, H. & Oerter, H.* (eds.) (1990): Die Expedition ANTARKTIS-V mit FS „Polarstern“ 1986/87, Bericht von den Fahrtabschnitten ANT-V/4-5.- *Berichte Polarforsch.* 57: 1-207.
- Moser, J.* (1991): Raum-Zeit-Variation der chemischen Zusammensetzung des Firns antarktischer Randgebiete.- Dissertation, Ruprecht-Karls-Universität, Heidelberg.
- Thyssen, F. & Grosfeld, K.* (1988): Ekström Ice-Shelf, Antarctica.- *Annals Glaciol.* 11: 180-183.
- Wright, D.L., Hodge, S.M., Bradley, J.A., Grover, T.P. & Jacobel, R.W.* (1990): A Digital Low-Frequency, Surface Profiling Ice-Radar System.- *J. Glaciol.* 36:
- Wu, T.T. & King, R.W.* (1965): The cylindrical antenna with nonreflecting resistive loading.- *IEEE Trans. Antennas and Propagation*, vol. AP-13: 369-373.

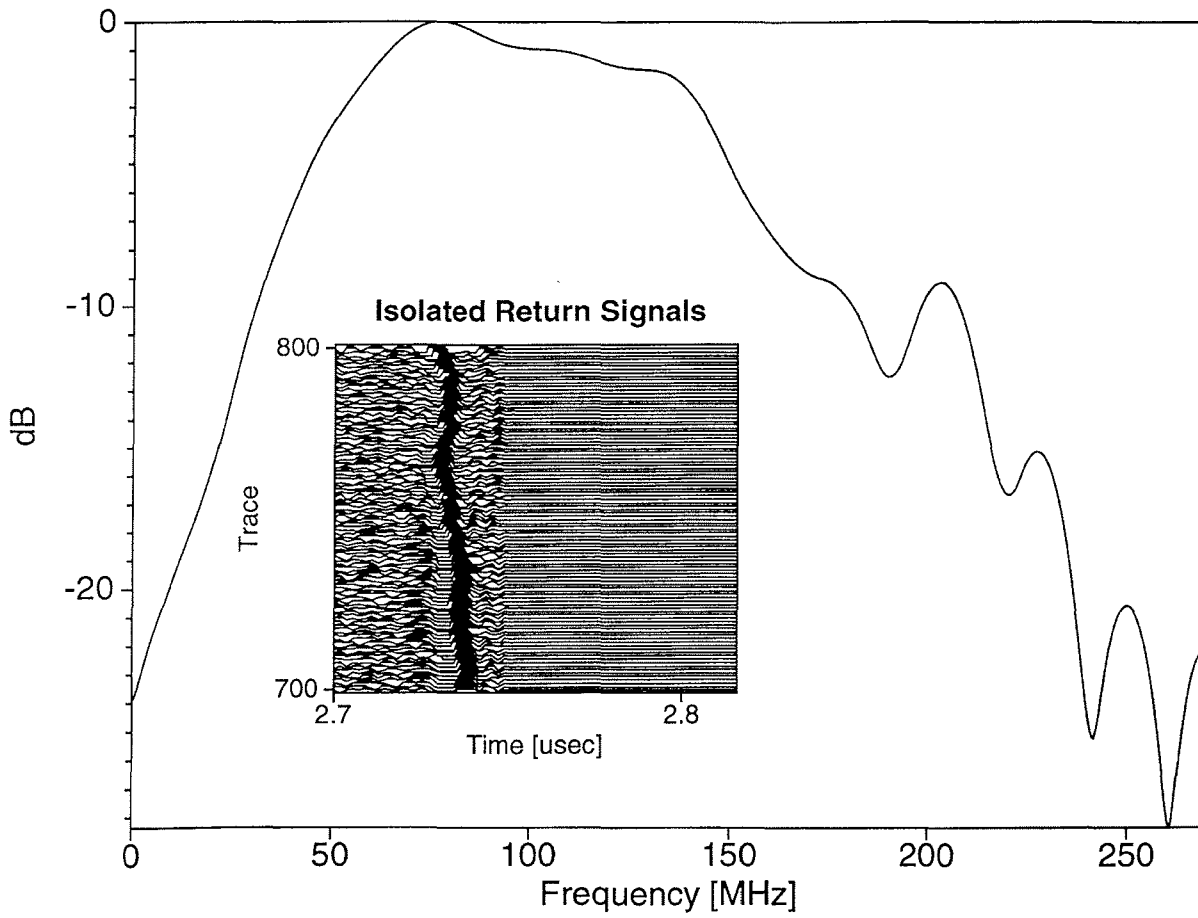


**Fig. 12:** Bandwidth of 100 Mhz antennas. The spectra of 100 bottom returns have been averaged to estimate bandwidth of the filter-chain and transmission path. The -3 dB bandwidth is about 90 MHz.

**Abb. 12:** Bandbreite der 100 MHz-Antennen. Die Spektren von 100 Bodenechos wurden gemittelt, um die Bandbreite des Gesamtsystems zu beurteilen. Die Bandbreite zwischen den -3 dB Punkten beträgt etwa 90 MHz.

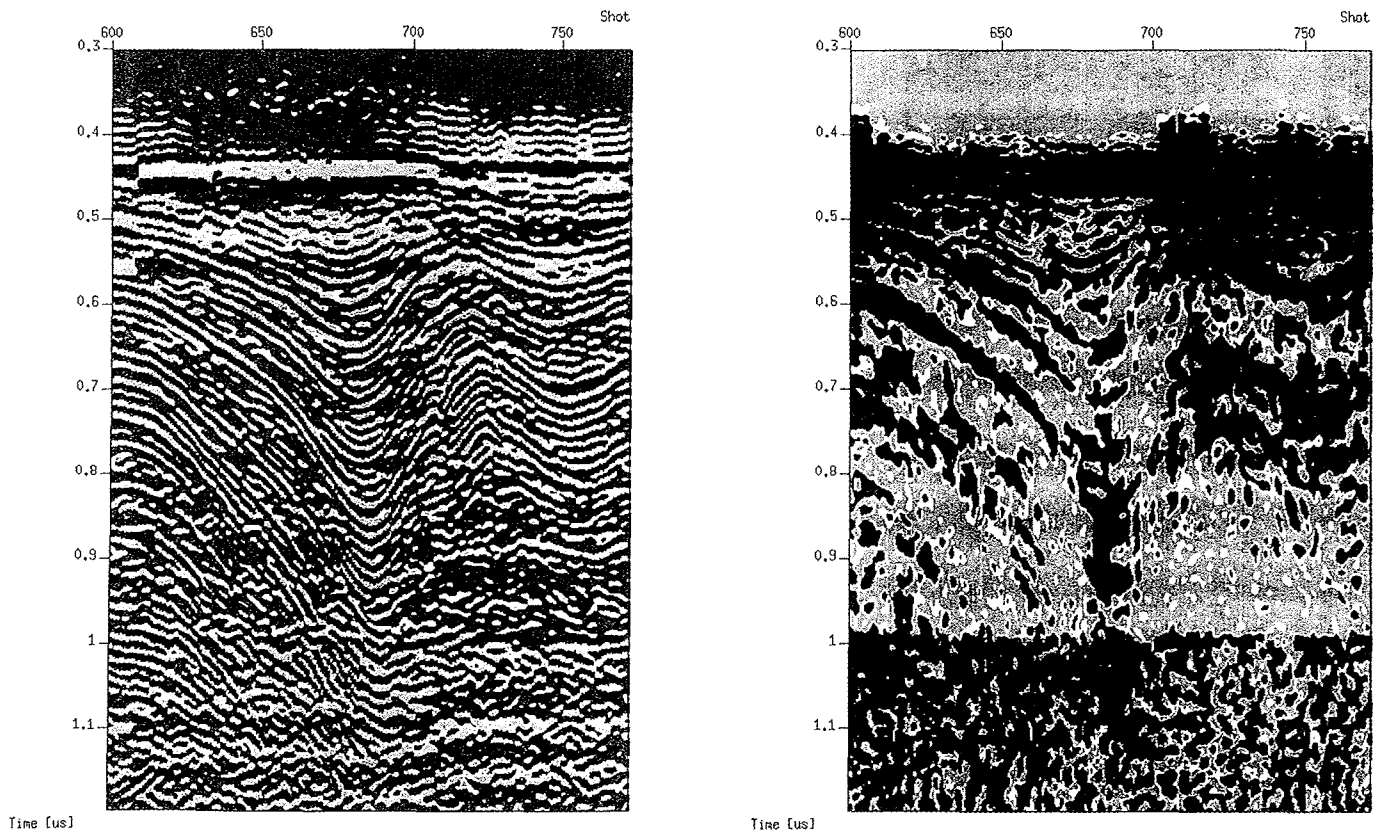


**Fig. 13:** Full waveform- (left panel) and envelope-representation (right panel). The apparently high-resolution image of the full waveform data is generated mostly by interference of individual waveforms. The envelope (right panel) is dependent on bandwidth only and gives a more realistic picture of resolution. However, structural information is the same in both representations.

**Abb. 13:** Wellenform- (links) und Einhüllenden- (rechts) Darstellung eines Profilausschnittes. Das scheinbar hochauflösende Abbild der Wellenform-Darstellung wird vorwiegend durch Interferenzen erzeugt. Die Einhüllenden-Darstellung gibt ein realistischeres Bild der tatsächlich erzielbaren Auflösung. Dennoch ist die strukturelle Information in beiden Darstellungsformen etwa gleich.